PROCEEDINGS, 45th Workshop on Geothermal Reservoir Engineering
Stanford University, Stanford, California, February 10-12, 2020
SGP-TR-216

Investigating Mechanical Interactions between Fractures and Fracture Propagation Patterns in an EGS Reservoir

Ayaka Abe and Roland N. Horne

Department of Energy Resources Engineering, Stanford University, 367 Panama St, Stanford, CA 94305, USA

aabe@stanford.edu

Keywords: enhanced geothermal systems, hydraulic fracturing, and numerical modeling

ABSTRACT

During hydraulic stimulation treatment in an EGS reservoir, it is suggested that new fractures are initiated from stimulated preexisting fractures and propagate through a reservoir. This phenomenon has been observed in laboratory-scale experiments and field-scale observations. This stimulation mechanism which includes both creating new fractures and stimulating preexisting natural fractures is called "mixed-mechanism stimulation". In the mixed-mechanism stimulation, a fracture propagation from a preexisting fracture and the interaction of newly formed fractures and preexisting fractures play an important role in a complex fracture network creation. Especially in an EGS reservoir, preexisting fractures are large and dominate in a fracture network. Hydraulic stimulation is performed in a less permeable geothermal reservoir, which could mean that the large number of preexisting fractures are poorly connected. To better understand the mechanical interaction between fractures, how newly formed fractures propagate in a reservoir, and how fluid flows in a fracture network, a numerical model based on fracture mechanics and fluid mechanics is needed.

In this study, we developed a physics-based numerical model that couples fluid flow between fracture surfaces, fracture deformation, and fracture propagation driven by fluid injection. We modeled propagation of a hydraulic fracture, shear stimulation of a preexisting fracture, and propagation of a wing crack driven by fluid injection. The objective was to investigate the effect of mechanical interaction between newly formed fractures and preexisting fractures on a fracture network creation during hydraulic stimulation treatment in an EGS reservoir. The numerical experiment results show that there are three fracture network patterns observed; 1) a hydraulic fracture crosses the preexisting fracture, and continues propagating, 2) a hydraulic fracture follows the preexisting fracture, and the preexisting fracture initiates only one wing crack, and 3) a hydraulic fracture follows the preexisting fracture, and the preexisting fracture initiates two wing cracks. Those results imply that higher injection pressure likely create a more complex fracture network with the existence of well-oriented fractures and lower injection pressure likely create a less complex fracture network with less flow path branching. The fracture network complexity is affected by the fracture intersection angle and the magnitude of stress shadow effects as well. Understanding the difference between the cases where only one wing crack propagates and two wing cracks propagates will be necessary to proceed this study. Also, preexisting fractures are expected to be distributed in a complex arrangement with varied orientations, size distributions, and heterogeneous connectivity in an actual EGS reservoir. Further study will be done on modeling a realistic reservoir containing numbers of fractures with a reasonable variation, and confirm the implications of this study and understand fracture network creation at a reservoir scale.

1. INTRODUCTION

Observations of microseismicity show that a complex fracture network is often created during a hydraulic stimulation treatment in an EGS reservoir. The main mechanism of reservoir permeability enhancement was long believed to be shear dilation of preexisting natural fractures. However, the facts that: 1) bottomhole pressure exceeded the least principal stress, 2) pressure limiting was observed, and 3) fluid injection from a wellbore was through a preexisting fracture in most of the EGS projects, suggest that newly formed fractures propagated in the reservoir during stimulation (McClure and Horne 2014). This stimulation mechanism including both creating new fractures and stimulating preexisting natural fractures is called as "Mixed-Mechanism Stimulation", originally suggested in the unconventional oil and gas industry (Weng 2015; Weng et al. 2011; Wu and Olson 2014) and later suggested to be the common stimulation mechanism in enhanced geothermal reservoirs (Jung 2013; Kamali and Ghassemi 2016; Mcclure 2014; McClure and Horne 2014; Norbeck et al., 2018).

The observation that a hydraulic fracture often follows a preexisting fracture and branches into multiple fractures, and makes a complex fracture network has long been observed since Warpinski and Teufel's (1987) mineback experiments. The resulting fracture network complexity is strongly influenced by the distribution of the preexisting natural fractures and in-situ stress state (Weng 2015). The mixed-mechanism stimulation is now widely accepted to model a hydraulic stimulation in geothermal reservoirs and unconventional oil and gas reservoirs (e.g. Kamali and Ghassemi 2016, 2018; Maxwell et al. 2013; Norbeck et al. 2018; Norbeck and Shelly 2018; Weng et al. 2011). In mixed-mechanism stimulation, it is suggested that new fractures are initiated from sheared preexisting natural fractures and propagate in the reservoir. In hydraulic stimulation in an EGS reservoir, the target formation is often granitoid which has high tensile strength. Because it is hard to initiate new fractures from a wellbore drilled into granitoid, injected fluid flows into preexisting natural fractures which then slide and dilate at a lower pressure than required for initiating a new fracture. Therefore it is likely that new fractures are created from the tips of stimulated preexisting natural fractures as stress concentrates at the crack tips (McClure and Horne 2014).

A fracture created from another fracture has been observed in laboratory-scale experiments (e.g. Abe and Horne 2020; Erdogan and Sih 1963; Zoback 2007) and field scale observations (De Joussineau et al. 2007; Mutlu and Pollard 2008; Thomas and Pollard 1993). The secondary fracture initiated from a sheared preexisting natural fracture is called a "wing crack" or a "splay fracture". Wing cracks found in rock are tensile fractures but they are different from a hydraulic fracture propagating from a wellbore because: 1) wing cracks are initiated from the tension field induced by shear slip of a preexisting natural fracture while hydraulic fractures are initiated from an injection well by fluid pressure; 2) wing cracks are curved cracks while hydraulic fractures propagate straight and perpendicularly to the least principal stress; and 3) tension forces to open wing cracks are supported both by fluid pressure and shear slip of a preexisting natural fracture while tension forces to open hydraulic fractures are supported only by fluid pressure.

The magnitude of fluid pressure necessary to initiate a wing crack within a well-oriented natural fracture can be less than the fluid pressure to create new hydraulic fractures (Kamali and Ghassemi 2016, 2018; Mutlu and Pollard 2008; Zoback and Lund Snee 2018). Also, it is suggested that wing cracks play an important role in the mixed-mechanism stimulation because they improve the fracture connectivity and supply much larger storativity and transmissibility than those of preexisting fractures in a reservoir (Abe and Horne, 2019). Therefore, propagation of wing cracks and shear stimulation of natural fractures need to be considered when modeling a realistic fracture network to characterize an enhanced geothermal reservoir.

As discussed so far, a fracture propagation from a preexisting fracture and the interaction between newly formed fractures and preexisting fractures play an important role in modeling a complex fracture network creation. Especially in an EGS reservoir, preexisting fractures are expected to be large and dominant in a fracture network. Hydraulic stimulation is performed in a less permeable geothermal reservoir, which could mean that the preexisting fractures are poorly connected. To better understand the mechanical interaction between fractures, how newly formed fractures propagate in a reservoir, and how fluid flows in a fracture network, a numerical model based on fracture mechanics and fluid mechanics is needed.

In this study, we developed a physics-based numerical model that couples fluid flow between fracture surfaces, fracture deformation, and fracture propagation driven by fluid injection. We modeled hydraulic fracture propagation, shear stimulation of a preexisting fracture, and a wing crack propagation driven by fluid injection to investigate the effect of mechanical interaction between newly formed fractures and preexisting fractures on a fracture network creation during hydraulic stimulation treatment in an EGS reservoir.

2. METHODOLOGIES

During the hydraulic stimulation treatment, injected fluid flows mainly between preexisting and newly created fracture surfaces because the permeability of the matrix rock is low. Given that the fluid pressure between fractures drives fracture deformation and propagation, in this study we coupled fluid flow between the fracture surfaces with fracture deformation and propagation. The numerical formulation for this framework was presented originally in Abe and Horne (2019).

2.1 Fracture Crossing or Following Decision

The numerical formulation to decide whether a propagating fracture crosses or follows a preexisting fracture was first presented in Abe et al. (2019). This method applies the criterion for fracture crossing proposed by Renshaw and Pollard (1995). This criterion explains that crossing will occur if the slip along the frictional interface does not occur. In the numerical formulation, the segment along the preexisting fracture within the fracture process zone, where there is a possibility to initiate a fracture on the opposite side of the preexisting fracture, is discretized. Once the fracture-chance segment is discretized, each element is examined according to whether it slips by the induced stress field of a propagating hydraulic fracture. Three possibilities can occur. In the first case, the propagating fracture crosses a preexisting fracture when the induced stress field ahead of a crack tip causes neither slip nor opening along a preexisting fracture. A second possibility is that the propagating fracture follows a preexisting fracture when the induced stress field occurring ahead of a crack tip causes slip or opening along the preexisting fracture inside the fracture process zone. Third, when a part of the fracture-chance segment slips or opens, the propagating fracture may either cross or follow the preexisting fracture.

2.2 Fracture Deformation

To model fracture deformation, we used Ritz et al's (2015) two-dimensional displacement discontinuity boundary element method (DDM) with integrated complementarity. DDM is a powerful method that is useful to compute the stress shadow effect, which is the stress field induced by the deformation of other nearby fractures in a computationally effective way because only the fractures are discretized. In the DDM, a fracture is discretized into elements with each element having its normal and shear stresses and normal and shear displacements. Normal stress σ_{nn}^{i} and shear stress σ_{ns}^{i} acting on the i-th element (i = 1 to N) of a fracture, are related to normal displacement D_n^j and shear displacement D_s^j for all other elements including itself by j = 1 to N.

$$\begin{bmatrix} \sigma_{nn}^{i} = A_{nn}^{ij} D_n^j + A_{ns}^{ij} D_s^j \\ \sigma_{ns}^{i} = A_{sn}^{ij} D_n^j + A_{ss}^{ij} D_s^j \end{bmatrix} \quad for\ i,j = 1\ to\ N\ , \tag{1}$$

where A_{nn}^{ij}, A_{ns}^{ij}, A_{sn}^{ij}, and A_{ss}^{ij} are the coefficient of influence from the DDM formulation by Crouch and Starfield (1983). By using the DDM formulation, the mechanical equilibrium is expressed as:

$$\text{Normal stress: } {\sigma_n}^f = {\sigma_n}^r + P_f + A_{nn} D_n + A_{ns} D_s, \tag{2}$$

and:

$$\text{Shear stress: } \quad {\sigma_s}^f = {\sigma_s}^r + A_{sn} D_n + A_{ss} D_s, \tag{3}$$

where ${\sigma_n}^r$ and ${\sigma_s}^r$ are the remote stresses, and ${\sigma_n}^f$ and ${\sigma_s}^f$ are the traction acting at the center of each boundary element. σ_n takes tension as positive, σ_s takes right lateral as positive, D_n is negative when it is open, and D_s is positive in left lateral by following Crouch and Starfield (1983).

The complementarity formulation is modified from the original formulation by Ritz et al., (2015) to include the mechanically induced stresses induced by previous slip on the fracture as:

$$D_n \leq 0 \ \perp \sigma_n \leq 0, \tag{4}$$

$$0 \leq -{\sigma_s}^f - f{\sigma'}_n + S_f \ \perp 0 \leq \Delta D_s^R, \tag{5}$$

and:

$$0 \leq \ \ {\sigma_s}^f - f{\sigma'}_n + S_f \ \perp 0 \leq \Delta D_s^L, \tag{6}$$

where ΔD_s is the change of the shear displacement induced due to the current shear slip which is expressed as ${\Delta D_s}^t = (\Delta D_s^L)^t - (\Delta D_s^R)^t$. ΔD_s is decomposed into the slip into the right lateral slip ΔD_s^R and the left lateral slip ΔD_s^L following Ritz et al., (2015).

2.3 Fracture Propagation

The stress intensity factors for mode I, K_I and mode II, K_{II} are given by:

$$K_I = 0.798 \frac{D_n E\sqrt{\pi}}{4(1-\nu^2)\sqrt{P}}, \tag{7}$$

and:

$$K_{II} = 0.798 \frac{D_s E\sqrt{\pi}}{4(1-\nu^2)\sqrt{P}}, \tag{8}$$

where D_n and D_s are the normal and shear displacements for a fracture tip element respectively, E is the Young's modulus, ν is Poisson's ratio , and P is the length of the fracture tip element (Olson 1991, Mériaux and Lister, 2002).

The fracture propagation trajectory can be calculated by the maximum circumferential stress theory (Erdogan and Sih 1963). Thomas and Pollard, (1993) rewrote the original equations and solved directly for θ_0 as:

$$\theta_0 = \sin^{-1}\left(\frac{K_{II}}{K_I}\cos\phi\right) - \tan^{-1}\left(3\frac{K_{II}}{K_I}\right). \tag{9}$$

Crack extension begins when the maximum circumferential stress reaches a critical, material-constant value.

$$\cos\frac{\theta_0}{2}\left[K_I \cos^2\frac{\theta_0}{2} + \frac{3}{2}K_{II}\sin\theta_0\right] \geq \ K_{IC}, \tag{10}$$

where θ_0 is the fracture propagating deirection, K_{IC} is the critical stress intensity factor (Ingraffea 1987). Thomas and Pollard (1993) showed through laboratory experiments that this method reproduce a smoothly curved crack path.

In the present work, a propagating wing crack is divided into small boundary elements. New elements are added when the propagation criteria is satisfied at the crack tip.

2.4 Fluid Flow between Fracture Surfaces

Hydraulic stimulation treatments are performed in a low permeability reservoir such as a geothermal reservoir. In this study, the permeability of matrix rock was considered to be negligible as hydraulic stimulation is performed in a low permeability reservoir for a short period. Although there are some limitations by not considering the matrix fracture mass and heat transfer, the model is computationally effective and appropriate for modeling fracture propagations which occur for a short time period.

Fluid flow in a fracture can be assumed as a single-phase flow. The unsteady-state fluid mass conservation equation in a fracture is:

$$\frac{\partial(\rho E)}{\partial t} = \nabla \cdot \left(q_{flux} E\right) + s_a, \tag{11}$$

where ρ is the fluid density, t is time, q_{flux} is mass flow rate per cross sectional area of flow , E is the aperture, and s_a is a source term (mass per time) such as well injection or production (Aziz and Settari, 1979). Fluid is assumed to flow in a fracture with smooth parallel plates. By using the cubic law, the same equation is derived by assuming Darcy's flow for the flow in porous media (Zimmerman et al., 1994). Assuming Darcy's flow in one dimension and applying the cubic law, q_{flux} is:

$$q_{flux} = -\frac{e^3 w\rho}{12\mu}\frac{\partial P}{\partial x_i}, \tag{12}$$

where μ is the fluid viscosity, and P is the fluid pressure. This expression is also known as the Plane Poiseuille flow which is the solution to the Navier-Stokes equation for the flow between those parallel plates. The Plane Poiseuille flow describes laminar flow

between two parallel plates (Zimmerman et al., 1994). Here we assumed the fluid density and viscosity are constants and do not depend on the temperature and pressure.

In this work, we employed the equation derived by Willis-Richards et al., (1996) to compute the aperture of a closed fracture. The aperture of a closed fracture is given by:

$$e = \frac{e_0}{1+9\sigma_n'/\sigma_{nref}} + D_s tan\frac{\varphi}{1+9\sigma_n'/\sigma_{nref}}, \quad (13)$$

where e_0 is the aperture at zero effective stress, φ is the dilation angle, σ_{nref} is the effective normal stress applied to cause a 90% reduction of aperture. Those parameters are derived through a laboratory measurement.

When the element opens, we assume that the total aperture is the sum of the normal displacement computed by DDM and the hydraulic aperture as:

$$E = D_n + e_0. \quad (14)$$

Fluid flow and fracture deformation are coupled by a fully implicit scheme. The Newton-Raphson method was used to solve the system of nonlinear equations as the transmissibility matrix and the accumulation term is nonlinear.

3. NUMERICAL EXPERIMENT SETUP

In this study, we modeled wing crack propagation from a stimulated preexisting fracture and hydraulic fracture propagation from a wellbore driven by fluid injection. We compared fracture propagation patterns when a propagating hydraulic fracture crosses a preexisting fracture and when a propagating hydraulic fracture stops at a preexisting fracture, in order to analyze the effects of stress state and mechanical interaction between fractures on the creation of the fracture network.

3.1 Parameters

The reservoir we modeled is a full space, horizontal, isotropic, and homogeneous two-dimensional domain with a vertical fracture assuming the plane strain condition. An injection well located at the center of the domain initiates a hydraulic fracture, then the propagating hydraulic fracture hits two preexisting natural fractures on its both sides. Those two preexisting natural fractures are located so that the fracture network will be symmetric.

In this study, we investigated the effects of stress states and fracture orientations on the creation of a fracture network pattern. The stress ratios were varied from 1.1 to 4.0 (Table 1) with the fixed value of $\sigma_h = 10$MPa. The fracture orientations used in this study are 45 and 60 degrees to the maximum horizontal stress orientation.

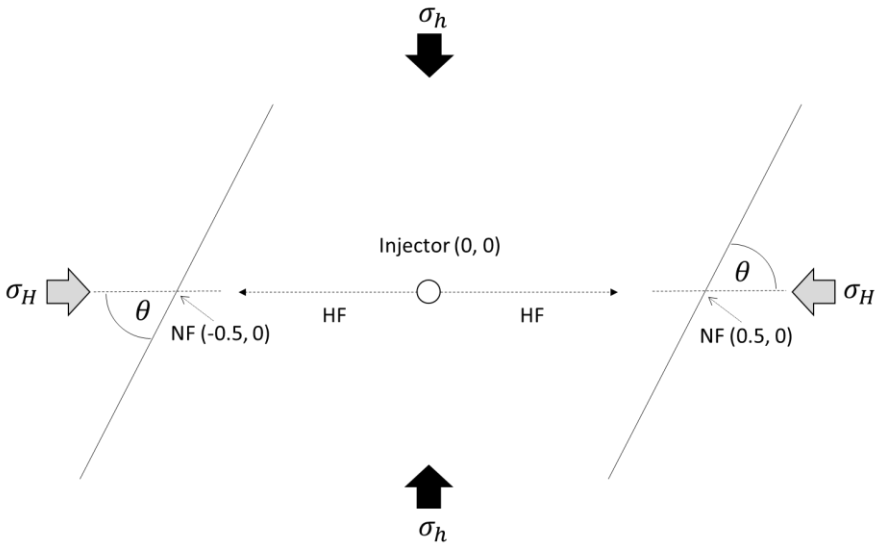

Figure 1: Simulation setup. An injection well located at the center of the domain initiates a hydraulic fracture (HF). Propagating hydraulic fracture intersects to a preexisting natural fracture (NF) at each side.

Table 1: The stress ratios and the fracture orientations compared in this study

Stress Ratio	$\frac{\sigma_H}{\sigma_h}$	1.1	2.0	3.0	4.0
Fracture Orientation	θ	45		60	

Table 2: Parameters used in the numerical simulation

Main fracture grid half length	1.25e-2	m
Preexisting fracture length	1.0	m
Wing crack grid half length	6.10e-3	m
Initial Time Step	1.0e-4	s
Injection/Production Rate	4.0e-6	m^3/s
Minimum horizontal stress	10	MPa
Initial fluid pressure	0	MPa
Critical stress intensity factor	0.39	MPa
Young's modulus	11.8	GPa
Poisson's ratio	0.21	-
Fracture height	1	m
Water density	920	kg/m^3
Water viscosity	1.0e-9	MPa.s
Reference hydraulic aperture	1.0e-4	m
Reference effective normal stress	25	MPa
Dilation angle	2	degree
Fracture static frictional coefficient	0.7	-
Fracture dynamic frictional coefficient	0.7	-
Frictional strength	0.0	MPa
Injection Duration	100	sec

3.2 Propagating Fracture Cross or Follow Decision

Fracture cross/follow conditions are determined based on the method described in Section 2.1. The fracture cross/follow conditions depend of the stress state, the frictional coefficient of the fracture, and the tensile strength of the rock. With the parameters given in Table 2, a propagating hydraulic fracture terminates at a preexisting fracture oriented at 45 degrees under all stress states in

Table 1. The stress states that induce slip without fluid injection were not included in this experiment.

The stress ratios over 4.0 make the propagating fracture cross the preexisting fracture oriented at 60 degrees, but the stress ratios below 4.0 make the condition where the propagating fracture may either cross or follow the preexisting fracture. "Cross or follow" in Table 3 means that there are both possibilities of cross or follow (Abe et al. 2019). In this experiment, we made the propagating fracture follow the preexisting fracture with the stress ratio 1.1, and made the propagating fracture cross with the stress ratio larger than 2.0 in this condition.

Table 3: Propagating Fracture Cross or Follow

Fracture Angle [degrees]	60			
Stress Ratio $\frac{\sigma_H}{\sigma_h}$	1.1	2.0	3.0	4.0
Propagating fracture cross/follow	Follow	Cross	Cross	Cross

Fracture Angle [degrees]	45			
Stress Ratio $\frac{\sigma_H}{\sigma_h}$	1.1	2.0	3.0	4.0
Propagating fracture cross/follow	Follow	Follow	Follow	Follow

4. RESULTS

4.1 Fracture Orientation of 60 degrees

When there is a preexisting fracture with a 60-degree orientation, a propagating fracture follows when the stress ratio is low, and crosses when the stress ratio is high. We modeled fracture propagation with varied stress ratios to compare the results for both scenarios: when a propagating fracture follows and when it crosses the preexisting fracture.

Figure 2 shows that the fracture propagation patterns differ by cross/follow cases. When a propagating fracture crosses the preexisting natural fracture, the propagating fracture continues to propagate while the natural fracture remains without slip or opening. On the other hand, when a propagating fracture follows the preexisting fracture, the side with the larger angle to the hydraulic fracture slips, while the other side does not (Figure 4). As a result, a wing crack initiates and propagates from the slip side of the preexisting fracture. In both cases, the fluid flow path mainly remains as one pathway, creating a less complex fracture network. The fluid pressures inside the fractures are almost uniform and close to the magnitude of the least horizontal stress.

Only one side of a preexisting fracture initiates a wing crack when the stress ratio is 1.1 is because the local stress field induced by the propagating fracture tip causes asymmetric normal and shear stress distributions along the preexisting fracture. Figure 3 compares the normal and shear stresses acting along the preexisting fractures. The side that initiates a wing crack (x = 0.5 m to 1.0 m) is under larger shear stresses and smaller normal stresses compared to the other side (x = 0.0 m to 0.5 m). This asymmetric stress distribution makes one side slip earlier than the other side despite the fluid pressure distribution being almost symmetric. A wing crack propagates at a lower fluid pressure than that needed to make the other side of the preexisting fracture slip with the result that only one wing crack propagates from each preexisting fracture.

When a propagating fracture crosses the preexisting fracture, the fluid pressure necessary to drive the hydraulic fracture propagation is lower than that needed to induce slip along the preexisting fracture. Therefore, the hydraulic fracture keeps propagating without branching into the preexisting fractures (Figure 2).

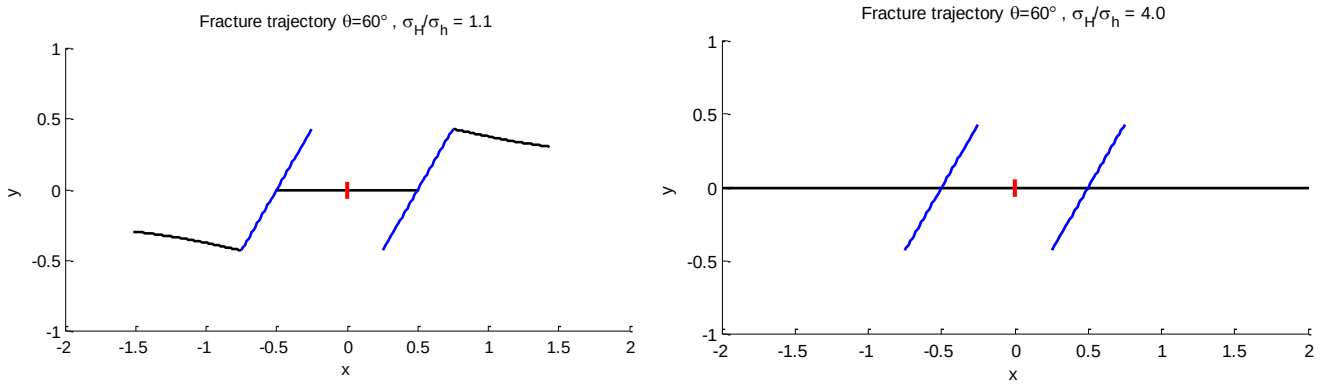

Figure 2: The fracture trajectories when the preexisting fractures are oriented at 60 degrees to the maximum horizontal stress. The red dot shows the location of the injection well, the blue lines are the preexisting fractures, while the black lines show the newly formed fractures including a hydraulic fracture initiated from the injection well and wing cracks.

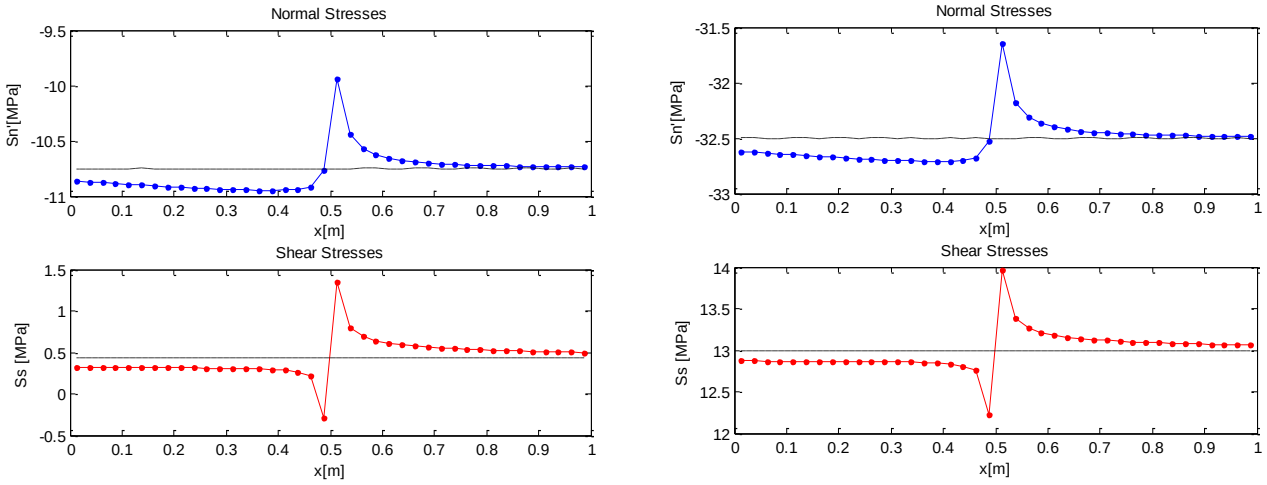

Figure 3: The normal stress and shear stress distribution along a preexisting fracture when a propagating fracture hits the preexisting fracture. The dot lines show the normal and shear stress by the remote stresses. Left: when the stress ratio is 1.1, Right: when the stress ratio is 4.0. The left plot shows that the side that initiates a wing crack (x = 0.5 m to 1.0 m) is under larger shear stresses and smaller normal stresses compared to the other side (x = 0.0 m to 0.5 m).

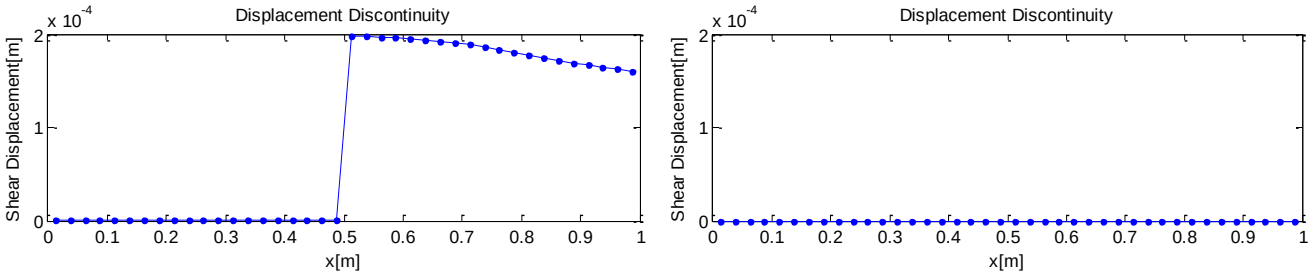

Figure 4: The shear displacements of a preexisting fracture. Left: when the stress ratio is 1.1, Right: when the stress ratio is 4.0. The left plot shows that the side that initiates a wing crack (x = 0.5 m to 1.0 m) has larger shear displacement while the other side has no shear displacement (x = 0.0 m to 0.5 m).

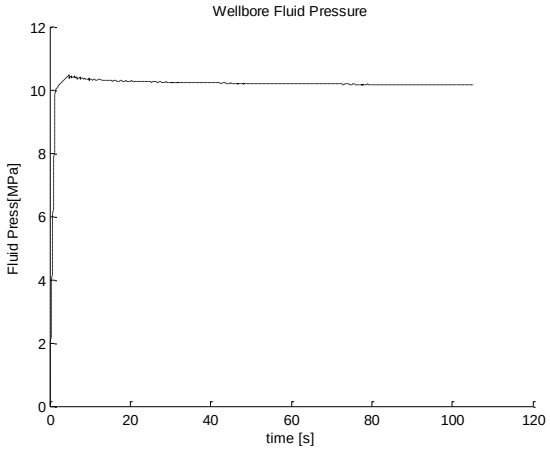

Figure 5: An example of the wellbore pressure when the stress ratio is 1.1.

4.2 Fracture Orientation of 45 degrees

We compared the fracture propagation patterns with different stress states for the fractures orienting at 45 degrees. For all the test cases, the propagating fracture cross/follow condition was "follow."

Figure 6 shows the fracture propagation patterns for cases with a stress ratio of 1.1 and 3.0. When the stress ratio is close to 1, a wing crack initiates from only one side of the preexisting fracture, with the same pattern as that we observed with a preexisting fracture oriented at 60 degrees. However, when the stress ratio is larger than 2.0, both sides of the preexisting fracture initiate wing cracks.

When the propagating hydraulic fracture intersects with the preexisting fractures, the fluid pressure inside is almost the same as the minimum horizontal stress. This means that the fluid pressure becomes sufficiently high to drive shear slip on the entire preexisting fracture when intersecting despite asymmetric stress distributions along the preexisting fracture. The slip induced by the injected fluid then becomes sufficiently high to initiate wing cracks on both sides. With a small stress ratio, the magnitude of the stress shadow effect is large relative to the stresses acting along the preexisting fracture. Therefore, the amount of shear slip is insufficient on the side that does not initiate a wing crack.

Once the preexisting fracture slips and initiates a wing crack, the wing crack propagation is driven by the shear slip at a certain length; later, the propagation is driven by the fluid pressure inside the wing crack (Kamali and Ghassemi 2018; Abe and Horne 2019). The fluid pressure to drive wing crack propagation is almost the same as the minimum horizontal stress because the fluid pressure necessary to propagate a mode I crack decreases as the crack lengthens (Anderson 2005; Zoback 2007).

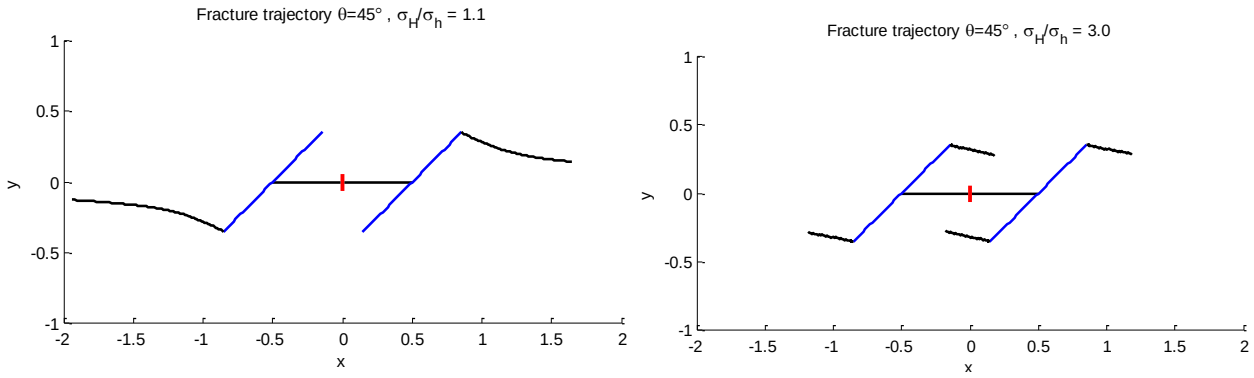

Figure 6: The fracture trajectories when the preexisting fractures are oriented at 45 degrees to the maximum horizontal stress. The red dot shows the location of the injection well, the blue lines are the preexisting fractures, while the black lines show the newly formed fractures including a hydraulic fracture initiated from the injection well and wing cracks.

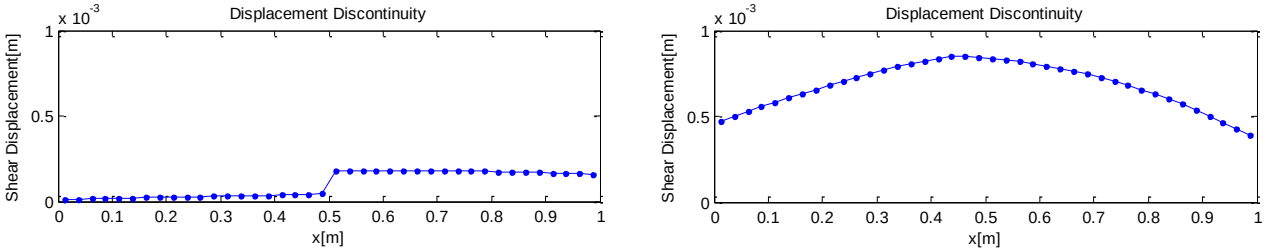

Figure 7: The shear displacements of a preexisting fracture. Left: when the stress ratio is 1.1, Right: when the stress ratio is 3.0. The left plot shows that the side that initiates a wing crack (x = 0.5 m to 1.0 m) has larger shear displacement compared to the other side (x = 0.0 m to 0.5 m). The right plot shows that although the side with larger angle toward the propagating hydraulic fracture has slightly larger magnitude of shear displacements than those of the other side, both sides slip sufficiently to initiate a wing crack.

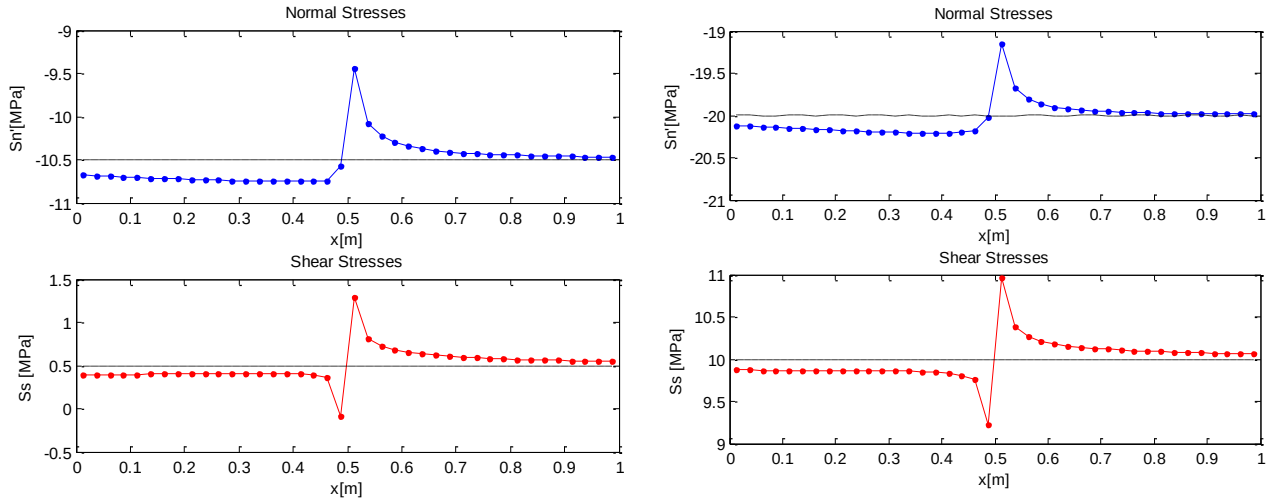

Figure 8: Shear stress and normal stress distribution along a preexisting fracture when a propagating fracture hits the preexisting fracture. The dot lines show the normal and shear stress by the remote stresses. Left: when the stress ratio is 1.1, Right: when the stress ratio is 3.0. The left plot shows that the side that initiates a wing crack (x = 0.5 m to 1.0 m) is under larger shear stresses and smaller normal stresses compared to the other side (x = 0.0 m to 0.5 m).

4.3 Comparison of Fracture Cross/Follow Pattern

Although a propagating fracture is supposed to follow the preexisting fractures oriented at 45 degrees based on the fracture cross/follow criteria (Table 3), it is not impossible that a propagating fracture still crosses the preexisting fracture because if a propagating fracture is

larger than the preexisting fracture, a propagating fracture could bypass the preexisting fracture in a three-dimensional setting (Fu et al. 2015), or if a preexisting fracture is partially cemented, fracture propagation may continue from the cemented regions (Fu et al. 2016).

We also compared the scenarios when a propagating fracture crosses the preexisting fracture oriented at 45 degrees. In these scenarios, the parameters used in the simulations are the same as those of the previous cases (Table 2), but the hydraulic fracture propagating from the injection well crosses the preexisting fracture when they intersect, and can propagate further if the fracture propagation criteria are satisfied.

The results show that even though the propagating hydraulic fracture crosses the preexisting fracture, the hydraulic fracture does not propagate further and wing cracks grow preferably instead (Table 4). Two wing cracks and the hydraulic fracture propagated simultaneously in only in one case with the stress ratio 2.0. These results suggest that the fracture propagation patterns are not strongly affected by the fracture cross/follow patterns for the four test cases in this study. When a propagating fracture crosses the preexisting fracture, the fluid pressure decreases around the intersection because the fluid flows into the preexisting fracture which has low initial fluid pressure. The fluid pressure that drives the shear slip along the preexisting fracture is lower than the pressure necessary to drive the crossed hydraulic fracture propagation in the case of fractures oriented at 45 degrees. Therefore, the fluid flow follows the preexisting fracture and wing cracks.

Although fracture cross/follow did not affect the three test cases in this study, this plays a critical role in determining the overall fracture network patterns. Also the experiment results by Beugelsdijk et al.,(2000) showed that injecting low viscosity fluid at a low injection rate made a fracture path that followed preexisting fractures and more branches because those fluids flow into preexisting fractures more easily than those of high viscosity. High viscosity fluid stayed in the hydraulic fracture and crossed the discontinuities and made a nearly straight fracture path. This might be because fracture bypassing occurred and fracture propagation continued from the site of the discontinuities, but these results suggest that fluid viscosity and injection rate are key factors of fracture cross/follow conditions as well.

In this study, we assumed the fracture height of propagating and preexisting fractures are the same. In future work, we will investigate further the cases where a propagating fracture height is larger than that of the preexisting fracture and will consider varied injection rate and viscosity.

Table 4: The summary of the results. "Only one wing crack" and "Two wing cracks" mean the fracture propagation pattern shown in Figure 6

Fracture Orientation θ	Cross/Follow Scenario	Stress Ratio $\frac{\sigma_H}{\sigma_h}$			
		1.1	2.0	3.0	4.0
45	Follow	Only one wing crack	Two wing cracks	Two wing cracks	Two wing cracks
45	Cross	Only one wing crack HF stops propagation	Two wing cracks HF continues propagation	Two wing cracks HF stops propagation	Two wing cracks HF stops propagation

5. DISCUSSION AND CONCLUSION

In this study, we modeled hydraulic stimulation in an EGS reservoir with two preexisting natural fractures. The model results show three fracture network patterns; 1) a hydraulic fracture crosses the preexisting fracture, and continues propagating, 2) a hydraulic fracture follows the preexisting fracture, and the preexisting fracture initiates only one wing crack, and 3) a hydraulic fracture follows the preexisting fracture, and the preexisting fracture initiates two wing cracks.

When a preexisting fracture slips, shear dilation and a wing crack propagation increase the volume to store fluid in the reservoir. This volume change causes a decrease of the fluid pressure inside the preexisting fracture. Hence, the injected fluid flows into the slipping fracture, creating a preferred flow path. Once the preexisting fracture slips and initiates a wing crack, the wing crack propagation is driven by the shear slip until it extends to a certain length; the propagation is then driven by the fluid pressure inside the wing crack (Kamali and Ghassemi 2018; Abe and Horne 2019). The length of a wing crack can be as long as the main preexisting fracture when it is well oriented. Most of the past EGS projects did not observe a propagating planar fracture perpendicular to the least principal stress unlike in an unconventional oil and gas reservoir. It is believed that preexisting fractures dominated the fracture network. Therefore, when a bottomhole pressure exceeds the least principal stress, it is highly likely that new fractures initiate from a preexisting fracture and propagate in a reservoir with the existence of well-oriented fractures.

Table 5: Summary of the results: The red dot shows the location of the injection well; the blue lines are the preexisting fractures, while the black lines show the newly formed fractures, including a hydraulic fracture initiated from the injection well and wing cracks.

Fracture Orientation θ	Stress Ratio $\frac{\sigma_H}{\sigma_h}$			
	1.1	2.0	3.0	4.0
60	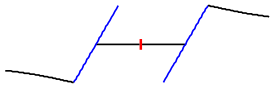	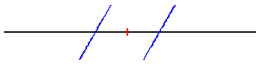	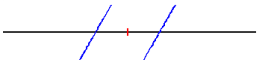	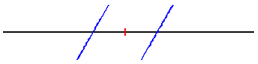
45	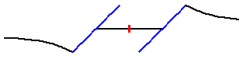	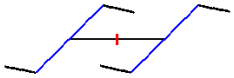	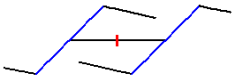	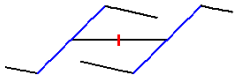

The fracture network patterns observed in this study are categorized into three different patterns, which can be described by Mohr's circle and the linearized Mohr–Coulomb failure envelope. Figure 9 shows the preexisting fracture orientations and stress states used in this study.

1) If a fracture sufficiently exceeds the Mohr–Coulomb failure envelope as a result of a hydraulic stimulation treatment, the entire preexisting fracture slips and initiates wing cracks from both edges. The fluid path then branches into two flow paths.

2) If a fracture slightly exceeds the Mohr–Coulomb failure envelope, the stress shadow effects induced by the intersecting upstream mode I fracture causes asymmetric normal and shear stress distributions along the preexisting fracture (Figure 3). The side with the larger angle to the propagating fracture is under larger shear stresses and smaller normal stresses compared to those of the other side. This asymmetric stress distribution results only one wing crack. A wing crack propagates at a lower fluid pressure than that needed to make the other side of the preexisting fracture slip with the result that only one wing crack propagates from each preexisting fracture.

3) If a fracture falls below the Mohr–Coulomb failure envelope, and when a propagating fracture crosses the preexisting fracture, the crossed propagating fracture continues propagating because the fluid pressure to drive the fracture propagation is lower than that needed to make the preexisting fracture slip. When a propagating fracture follows the preexisting fracture, the injected fluid increases its pressure until the preexisting fracture slips and initiates a wing crack. As a result, the pre-existing fracture slightly exceeds the Mohr–Coulomb failure envelope and becomes the state 2).

Table 6 shows the magnitude of the shear stress drop after a hydraulic fracture intersects with the preexisting fracture. The shear stress drop is expressed as $\Delta\sigma_s = \left|{\sigma_s}^f\right| - (-f{\sigma'}_n + S_f)$, where ${\sigma_s}^f$ is the shear stress, f is the frictional coefficient, ${\sigma'}_n$ is the effective normal stress, S_f is cohesion, and $(-f{\sigma'}_n + S_f)$ expresses the frictional strength. When the magnitude of the stress shadow effect is close to that of this stress drop, only one side of the preexisting fracture slips and initiates a wing crack. The magnitude of the stress shadow effect depends on the fracture size, the fracture-intersecting angle, and the effective normal stress acting on the fracture. The larger the fracture size or the effective normal stress the larger the stress shadow effect. The negative stress drop means that the fracture does not slip at the current fluid pressure. Instead, the fluid pressure needs to increase to induce slip along the preexisting fracture or fluid flows into another preferred path.

These results indicate that the fractures below the Mohr–Coulomb failure envelope likely have a smaller contribution to the fracture network creation and reservoir permeability enhancement. The fractures that are not critically stressed are often partially or entirely cemented because they were created a long geologic time ago in most cases. On the other hand, fractures with sufficient stress drop when stimulated have shear displacements that lead to shear dilation and eventually wing crack initiations from the edges. Those fractures likely dominate a fracture network and contribute to reservoir permeability enhancement.

The implications from the results of the eight cases in this study are as follows:

- Fractures sufficiently exceeding the Mohr–Coulomb failure envelope increase the number of flow paths and create a complex fracture network.
- Fractures not exceeding the Mohr–Coulomb failure envelope neither enhance their permeability nor create new fractures.
- Higher injection pressure can create a more complex fracture network in the presence of well-oriented fractures.
- Lower injection pressure may create a less complex fracture network with less flow path branching.

The stress state and fracture cross/follow condition also play a critical role in the fracture network complexity. However, the results suggest that injection pressure may also control the fracture network complexity.

In an actual EGS reservoir, preexisting fractures are expected to be distributed in a complex pattern with varied orientations, size distributions, and fracture connectivity; however, the simple reservoir setting in this study is reasonable to help us understand how preexisting fractures and newly formed fractures interact with each other to create a fracture network. This is because this numerical

physic-based model handles fluid flow between fracture surfaces, shear dilation of a preexisting fracture, fracture propagation, and mechanical interactions between fractures.

In future work, we will model a realistic reservoir containing a number of fractures with reasonable variation, to confirm the implications of this study and better understand fracture network creation at a reservoir scale.

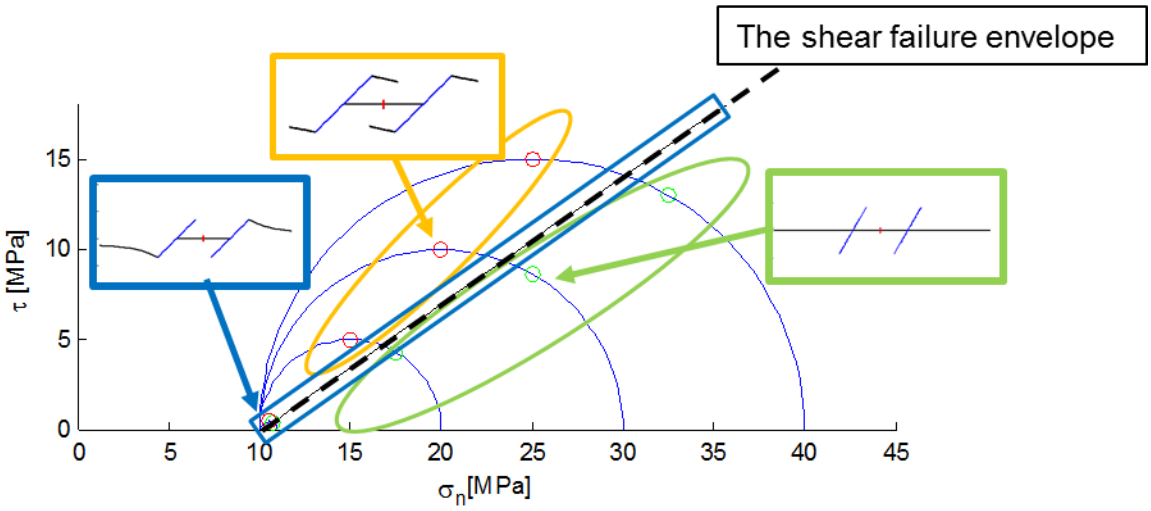

Figure 9: Mohr's circle showing the fractures and stress states used in this study. The black line shows the linearized Mohr–Coulomb failure envelope with fluid pressure at 10MPa. Green dots show the fracture orienting at 60 degrees, while red dots show the fractures orienting at 45 degrees.

Table 6: Shear stress drop $\Delta\sigma_s$ in MPa in each test case where $\Delta\sigma_s = |\sigma_s{}^f| - (-f\sigma'_n + S_f)$. The negative stress drop means the fracture does not slip at the current fluid pressure.

Fracture Orientation θ	Stress Ratio $\frac{\sigma_H}{\sigma_h}$			
	1.1	2.0	3.0	4.0
60	-0.092	-0.92	-1.84	-2.76
45	0.15	1.5	3.0	4.5

In almost all EGS projects, fluid was injected into a preexisting fracture intersecting with the injection well, with the result that the injection pressure exceeded the least principal stress (McClure and Horne, 2014). This observation and the results of this study support mixed-mechanism stimulation and the possibility of new fractures being formed from preexisting fractures.

In the Fenton Hill EGS project, it was observed that Massive Hydraulic Fracture (MHF) treatment, formed a broad microseismic cloud roughly 200 m wide, 1000 m long, and 1000 high. The estimated dominant preexisting fracture orientation toward the least principal stress was 53 degrees. The MHF treatment was performed at extremely high net-pressures of over 70 MPa, for 60 hours for most of the treatment. The fluid injection pressure exceeding 70MPa was sufficient to open the preexisting fractures (Brown et al., 2012; Norbeck, et al., 2018). This implies that a complex fracture network was created by the mixed-mechanism stimulation because the stress drop induced maximum shear displacement resulting in the entire fracture slipping at the fluid pressure opening preexisting fractures. It is likely that a flow path from the injection well branched as it intersected a preexisting fracture, which resulted in forming a broad microseismic cloud.

In this study, we initiated a hydraulic fracture from an injection well in this study. However, because fluid injection from a wellbore flows through a preexisting fracture in most of the EGS projects (McClure and Horne, 2014), our future work will investigate scenarios in which the fluid is injected into a preexisting fracture causing wing cracks to propagate and intersect with another preexisting fracture. Here, we suggested that the magnitude of stress drop affects fracture propagation patterns. These are also affected by the fracture intersection angle and the magnitude of stress shadow effects. To uncover the causes leading to fracture propagation patterns, it will first be necessary to understand the difference between the cases where only one wing crack is propagated vs. two wing cracks being propagated. Furthermore we will work on modeling a realistic reservoir containing a number of reasonably varied fractures, this will enable us to confirm the implications of the present study and better understand fracture network creation at a reservoir scale.

6. ACKNOWLEDGEMENTS

This research was supported by the Ito Foundation for International Education Exchange, by Ms. Margot Leidig through the grant of the Calvin Enderlin Earth Sciences Fellowship, and by the industrial affiliates of the Stanford Center for Induced and Triggered Seismicity.

REFERENCES

Abe, Ayaka and Roland N. Horne. 2019. "Investigating the Effect of Wing Cracks on the EGS Reservoir Permeability Enhancement by Hydraulic Stimulation." *American Rock Mechanics Association*.

Abe, Ayaka and Roland N. Horne. 2020. "Experimental Investigation on Fracture Network Creation by Hydraulic Stimulation." Pp. 1–9 in *Proceedings World Geothermal Congress*. Reykjavik, Iceland.

Abe, Ayaka, Takuya Ishibashi, Hiroshi Asanuma, and Roland N. Horne. 2019. "Numerical Modeling and Laboratory Experiments on a Propagating Hydraulic Fracture Intersecting with a Preexisting Fracture." Pp. 1–15 in *PROCEEDINGS, 43rd Workshop on Geothermal Reservoir Engineering Stanford University*. Stanford, California.

Anderson, Ted L. 2005. *Fracture Mechanics – Fundamentals and Applications*. Third edit. Boca Raton: CRC Press.

Aziz, Khalid and Antonín Settari. 1979. *Petroleum Reservoir Simulation*. Applied Science Publishers.

Beugelsdijk, L. J. L., C. J. De Pater, and K. Sato. 2000. "Experimental Hydraulic Fracture Propagation in a Multi-Fractured Medium." *Proceedings of the SPE Asia Pacific Conference on Integrated Modelling for Asset Management* 177–84.

Brown, Donald W., David V. Duchane, Grant Heiken, and Vivi Thomas Hriscu. 2012. *Mining Earth's Heat-Hot Dry Rock Geothermal Energy*. Berlin, Heidelberg: Springer Berlin Heidelberg.

Crouch, Steven L. and A. M. Starfield. 1983. *Boundary Element Methods in Solid Mechanics : With Applications in Rock Mechanics and Geological Engineering*. London ; Allen & Unwin.

Erdogan, F. and G. C. Sih. 1963. "On the Crack Extension in Plates Under Plane Loading and Transverse Shear." *Journal of Basic Engineering* 85(4):519–25.

Fu, P., L. Cruz, D. Moos, R. R. Settgast, and F. J. Ryerson. 2015. "Numerical Investigation of a Hydraulic Fracture Bypassing a Natural Fracture in 3D."

Fu, Wei, Brandon C. Ames, Andrew P. Bunger, and Alexei A. Savitski. 2016. "Impact of Partially Cemented and Non-Persistent Natural Fractures on Hydraulic Fracture Propagation." *Rock Mechanics and Rock Engineering* 49:4519–26.

Ingraffea, Anthony R. 1987. "3.Theory of Crack Initiation and Propagation in Rock." in *Fracture Mechanics*, edited by B. K. Atkinson.

De Joussineau, Ghislain, Ovunc Mutlu, Atilla Aydin, and David D. Pollard. 2007. "Characterization of Strike-Slip Faultesplay Relationships in Sandstone."

Jung, Reinhard. 2013. "EGS — Goodbye or Back to the Future." Pp. 95–121 in *Effective and Sustainable Hydraulic Fracturing*.

Kamali, Amirhossein and Ahmad Ghassemi. 2016. "Analysis of Natural Fracture Shear Slip and Propagation in Response to Injection." *PROCEEDINGS Geothermal Reservoir Engineering Stanford University*.

Kamali, Amirhossein and Ahmad Ghassemi. 2018. "Analysis of Injection-Induced Shear Slip and Fracture Propagation in Geothermal Reservoir Stimulation." *Geothermics* 76:93–105.

Maxwell, S. C., X. Weng, O. Kresse, and J. Rutledge. 2013. "Modeling Microseismic Hydraulic Fracture Deformation." in *SPE Annual Technical Confeence*.

Mcclure, Mark W. 2014. "Stimulation Mechanism and the Direction of Propagation of Microseismicity." *PROCEEDINGS, Thirty-Ninth Workshop on Geothermal Reservoir Engineering Stanford University*.

McClure, Mark W. and Roland N. Horne. 2014. "An Investigation of Stimulation Mechanisms in Enhanced Geothermal Systems." *International Journal of Rock Mechanics and Mining Sciences* 72:242–60.

Mériaux, Catherine and John R. Lister. 2002. "Calculation of Dike Trajectories from Volcanic Centers." *Journal of Geophysical Research: Solid Earth* 107(B4):ETG 10-1-ETG 10-10.

Mutlu, Ovunc and D. D. Pollard. 2008. "On the Patterns of Wing Cracks along an Outcrop Scale Flaw: A Numerical Modeling Approach Using Complementarity." *Journal of Geophysical Research: Solid Earth* 113(6):1–20.

Norbeck, Jack H., Mark W. McClure, and Roland N. Horne. 2018. "Field Observations at the Fenton Hill Enhanced Geothermal System Test Site Support Mixed-Mechanism Stimulation." *Geothermics* 74(February):135–49.

Norbeck, Jack H. and David R. Shelly. 2018. "Exploring the Role of Mixed-Mechanism Fracturing and Fluid-Faulting Interactions During the 2014 Long Valley Caldera, California, Earthquake Swarm." in *PROCEEDINGS Geothermal Reservoir Engineering Stanford University*.

Olson, Jon Edward. 1991. "Fracture Mechanics Analysis of Joints and Veins." Stanford University.

Ritz, Elizabeth, David D. Pollard, and Michael Ferris. 2015. "The Influence of Fault Geometry on Small Strike-Slip Fault Mechanics."

Thomas, Andrew L. and David D. Pollard. 1993. "The Geometry of Echelon Fractures in Rock: Implications from Laboratory and Numerical Experiments." *Journal of Structural Geology* 15(3–5):323–34.

Warpinski, N. R. and L. W. Teufel. 1987. "Influence of Geologic Discontinuities on Hydraulic Fracture Propagation." *Journal of*

Petroleum Technology 39(02):209–20.

Weng, X. 2015. “Modeling of Complex Hydraulic Fractures in Naturally Fractured Formation.” *Journal of Unconventional Oil and Gas Resources* 9:114–35.

Weng, X., O. Kresse, C. Cohen, R. Wu, and H. Gu. 2011. “Modeling of Hydraulic-Fracture-Network Propagation in a Naturally Fractured Formation.”

Willis-Richards, J., K. Watanabe, and H. Takahashi. 1996. “Progress toward a Stochastic Rock Mechanic Model of Engineered Geothermal Systems.” *JOURNAL OF GEOPHYSICAL RESEARCH* 101(88):17, 481–17, 496.

Wu, Kan and Jon E. Olson. 2014. “Mechanics Analysis of Interaction Between Hydraulic and Natural Fractures in Shale Reservoirs.” *Proceedings of the 2nd Unconventional Resources Technology Conference* (January).

Zimmerman, Robert W., Gudmmdur S Bodvarsson, and Gudmundwr S Bodvarsson. 1994. “Hydraulic Conductivity of Rock Fractures.”

Zoback, Mark D. 2007. *Reservoir Geomechanics*. Cambridge University Press.

Zoback, Mark D. and Jens-Erik Lund Snee. 2018. “Predicted and Observed Shear on Preexisting Faults during Hydraulic Fracture Stimulation.” 3588–92.